Discovery of an Ultraviolet Counterpart to an Ultrafast X-Ray Outflow in the Quasar PG 1211+143

Gerard A. Kriss[1] , Julia C. Lee[2,3] , Ashkbiz Danehkar[2] , Michael A. Nowak[4] , Taotao Fang[5] ,
Martin J. Hardcastle[6] , Joseph Neilsen[7] , and Andrew Young[8]

[1] Space Telescope Science Institute, 3700 San Martin Drive, Baltimore, MD 21218, USA
[2] Harvard-Smithsonian Center for Astrophysics, 60 Garden Street, Cambridge, MA 02138, USA
[3] Harvard University, John A. Paulson School of Engineering & Applied Science, 29 Oxford Street, Cambridge, MA 02138, USA
[4] Massachusetts Institute of Technology, Kavli Institute for Astrophysics, Cambridge, MA 02139, USA
[5] Xiamen University, Department of Astronomy, Xiamen, Fujian 361005, People's Republic of China
[6] University of Hertfordshire, School of Physics, Astronomy and Mathematics, Hatfield, Hertfordshire AL10 9AB, UK
[7] Villanova University, Mendel Hall, Room 263A, 800 E. Lancaster Avenue, Villanova, PA 19085, USA
[8] University of Bristol, School of Physics, HH Wills Physics Laboratory, Bristol BS8 1TH, UK

Abstract

We observed the quasar PG 1211+143 using the Cosmic Origins Spectrograph on the *Hubble Space Telescope* in 2015 April as part of a joint campaign with the *Chandra X-ray Observatory* and the Jansky Very Large Array. Our ultraviolet spectra cover the wavelength range 912–2100 Å. We find a broad absorption feature ($\sim$1080 km s^{-1}) at an observed wavelength of 1240 Å. Interpreting this as H I Lyα, in the rest frame of PG 1211+143 ($z = 0.0809$), this corresponds to an outflow velocity of $-16{,}980$ km s^{-1} (outflow redshift $z_{\rm out} \sim -0.0551$), matching the moderate ionization X-ray absorption system detected in our *Chandra* observation and reported previously by Pounds et al. With a minimum H I column density of $\log N_{\rm H\,I} > 14.5$, and no absorption in other UV resonance lines, this Lyα absorber is consistent with arising in the same ultrafast outflow as the X-ray absorbing gas. The Lyα feature is weak or absent in archival ultraviolet spectra of PG 1211+143, strongly suggesting that this absorption is transient, and intrinsic to PG 1211+143. Such a simultaneous detection in two independent wavebands for the first time gives strong confirmation of the reality of an ultrafast outflow in an active galactic nucleus.

Key words: galaxies: active – galaxies: individual (PG 1211+143) – galaxies: nuclei – galaxies: Seyfert

1. Introduction

Fast, massive outflows from active galactic nuclei (AGNs) may play a prominent role in the evolution of their host galaxies. These outflows may both heat and remove the interstellar medium (ISM) of the host galaxy, effectively stopping further star formation, and removing the fuel for further black hole growth (Silk & Rees 1998; King 2003; Ostriker et al. 2010; Soker 2010; Faucher-Giguère & Quataert 2012; Zubovas & Nayakshin 2014; Thompson et al. 2015). If the kinetic luminosity is high enough, 0.5% (Hopkins & Elvis 2010) to 5% (Di Matteo et al. 2005) of the bolometric luminosity, then the impact on the host galaxy may be sufficient to regulate galaxy growth and produce the observed $M_{\rm BH}$–$\sigma_{\rm bulge}$ correlation (Ferrarese & Merritt 2000; Gebhardt et al. 2000). Recent observations of high-luminosity AGNs at moderate redshifts demonstrate that outflows of this power, spanning galactic scales do exist (Borguet et al. 2013), and that such outflows may be ubiquitous, even when not seen in absorption along the line of sight (Liu et al. 2013a, 2013b, 2014).

Outflows implied by the X-ray warm absorbers and blueshifted UV absorption lines commonly seen in nearby AGNs (Crenshaw et al. 2003) are often too weak to potentially influence their host galaxies (Crenshaw & Kraemer 2012). On the other hand, ultrafast outflows (UFOs), typified by high column densities of highly ionized gas and primarily identified via Fe XXVI Kα absorption outflowing at velocities of >10,000 km s^{-1} would have the mass and kinetic energy to make a substantial impact on the evolution of their hosts (Pounds et al. 2003; Tombesi et al. 2010; Tombesi & Cappi 2014; King &

Pounds 2015). However, given the low statistical significance of these features and the fact that they are often based on the identification of only a single spectral feature, Vaughan & Uttley (2008) have questioned their reality. The large, comprehensive warm absorbers in the X-ray survey (Laha et al. 2014) found no significant statistical evidence for UFOs in the six sources they had in common with Tombesi et al. (2010). While not discussing the data per se, Gallo & Fabian (2013) argue for an alternative explanation based on blurred reflection rather than an outflowing wind.

The quasi-stellar object (QSO) PG 1211+143 ($z = 0.0809$) plays a central role in the controversy over relativistic outflows because it presents tantalizing evidence for the presence of UFOs and both intermediate and lower-velocity flows typical of warm absorbers. Pounds et al. (2003, 2016) identified two UFOs: one at high velocity $v_{\rm out} \sim -0.14c$, but also a lower-velocity UFO at $v_{\rm out} \sim -0.06c$.[9] However, studying the same original *XMM* observation of PG 1211+143 as Pounds et al. (2003), Kaspi & Behar (2006) find no evidence for UFOs, but rather lower-velocity systems more typical of those seen in warm absorbers. Pounds & Reeves (2009) and Tombesi et al. (2011) find UFOs persistently present, but varying in strength over the course of several *XMM* observations, spanning months to years, while a long, 300 ks NuSTAR observation of PG 1211 +143 also finds no evidence for UFOs (Zoghbi et al. 2015).

Prior UV spectra of PG 1211+143 revealed the usual blue continuum and broad emission lines typical of a Type 1 AGN,

---

[9] We use the convention that the velocities given in prior work on PG 1211 +143 are relativistic velocities in its rest frame, with $v_{\rm out}$ represented as zc simply by dividing $v_{\rm out}$ by $c = 2.9979 \times 10^5$ km s^{-1}.

Table 1
HST/COS Observations of PG 1211+143

Proposal ID	Data Set Name	Grating/Tilt	Date	Start Time (GMT)	Exposure (s)
13947	lcs501010	G140L/1280	2015 Apr 12	15:50:03	1900
13947	lcs504010	G140L/1280	2015 Apr 14	13:52:21	1900
13947	lcs502010	G140L/1280	2015 Apr 14	15:36:39	1900
13947	lcs502020	G130M/1327	2015 Apr 14	17:16:34	2320

but no absorption lines typical of the outflows seen in other AGNs. All absorption lines in the spectrum (including ones at velocities near that of the $v_{out} \sim -0.06\,c$ X-ray absorber) were identified as intervening gas in the intergalactic medium (IGM; Penton et al. 2004; Tumlinson et al. 2005; Danforth & Shull 2008; Tilton et al. 2012). Given the variety of results obtained on PG 1211+143 and its prominence in the controversy over the reality of high-velocity outflows in AGNs, we undertook a large joint campaign using the *Chandra* X-ray Observatory, the *Hubble Space Telescope* (*HST*), and the Karl G. Jansky Very Large Array (VLA) to search for both X-ray and ultraviolet outflowing absorption systems. We report on the *HST* UV results here. See Danehkar et al. 2018 for the *Chandra* HETGS X-ray results complementing this paper. As in Danehkar et al. (2018), in this paper, we will use the following conventions for velocities and redshift:

$z_{rest} = 0.0809$ defines the rest frame of PG 1211+143.
z_{obs} is the observed redshift of a spectral feature in our reference frame.
z_{out} gives the redshift of an outflow in the rest frame of PG 1211+143.
v_{out} gives the velocity of an outflow in the rest frame of PG 1211+143.
λ_{obs} is the observed wavelength of a spectral feature.
λ_0 is the rest wavelength (vacuum) of a spectral feature.

The usual special relativistic relations are used for conversions among the various quantities:

$z_{obs} = (\lambda_{obs}/\lambda_0) - 1$,
$z_{out} = (1 + z_{obs})/(1 + z_{rest}) - 1$,
$v_{out} = c[(1 + z_{out})^2 - 1]/[(1 + z_{out})^2 + 1]$, and
$z_{out} = \sqrt{[(1 + v_{out}/c)/(1 - v_{out}/c)]} - 1$, where c is the speed of light.

2. *HST* Observations

In 2015 April, we observed PG 1211+143 using *Chandra* and *HST* in a coordinated set of visits. The *HST*/COS observations used grating G140L with a central wavelength setting of 1280 to cover the entire 912–2000 Å wavelength range (Green et al. 2012). The COS data are available in the MAST archive at 10.17909/T9XQ1M . To fill in the gap in wavelength coverage between segments A and B of the COS detector, in our second visit we also used grating G130M with a central wavelength setting of 1327 Å. The observations are summarized in Table 1. All observations were split into four exposures at different FP-POS positions to enable us to remove detector artifacts and flat-field features.

The individual exposures in our program were combined by grating with updated wavelength calibrations, flat-fields, and flux calibrations using the methods of Kriss et al. (2011) and De Rosa et al. (2015). To adjust the wavelength zero points of
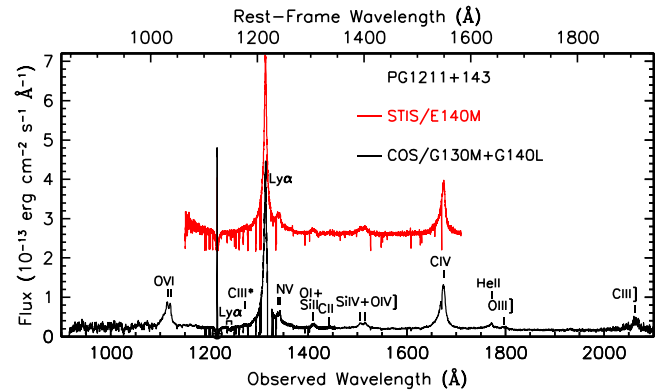

Figure 1. Merged *HST*/COS G130M and G140L spectra of PG 1211+143 (black) compared to the 2002 STIS/E140M spectrum (red). Wavelengths on the lower horizontal axis and fluxes are observed units. The upper horizontal axis shows wavelengths in the rest frame of PG 1211+143 at $z = 0.0809$. For clarity, the STIS spectrum has been offset vertically by 2.2×10^{-13} erg cm^{-2} s^{-1} Å^{-1}. Prominent emission lines are marked. An earth symbol denotes the strong geocoronal Lyα emission line. All narrow absorption features are either foreground ISM or IGM absorption lines. The broad Lyα absorption feature in the COS spectrum is marked above the spectrum in the blue wing of the Lyα emission line.

our spectra, for G130M, we cross-correlated our spectra with the archival STIS spectrum of PG 1211+143 (Tumlinson et al. 2005). For G140L, we measured the wavelengths of low-ionization interstellar lines and molecular hydrogen features and compared them to the H I velocity of $v_{LSR} = -17$ km s^{-1} (Wakker et al. 2011). No adjustment to the G140L wavelengths was required.

Our *HST* observations showed PG 1211+143 to be similar in appearance to archival *HST* and IUE observations as shown in Figure 1. The continuum flux at 1350 Å rest (1465 Å observed) was $f_\lambda = 2.2 \times 10^{-14}$ erg cm^{-2} s^{-1} Å^{-1}, slightly below the historical median flux of 2.9×10^{-14} erg cm^{-2} s^{-1} Å^{-1}. Despite the lower flux and our shorter observation time, the signal-to-noise ratio (S/N) of our observation ($\sim$29 per resolution element for G130M at 1240 Å) significantly improved upon the prior 25-orbit STIS echelle spectrum. Since the goal of our observations was to look for evidence of outflowing gas in PG 1211+143 as evidenced by blueshifted absorption lines, we scrutinized our spectra carefully. This revealed a previously unknown weak, broad feature in the blue wing of the Lyα emission line as shown in Figure 2 and the upper panel of 3.

Although weak, narrow interstellar and intergalactic absorption lines have been previously cataloged in this region (Penton et al. 2004; Tumlinson et al. 2005; Danforth & Shull 2008; Tilton et al. 2012), this broad dip centered at $\sim$1240 Å was not readily visible in prior *HST* spectra. To convince ourselves that this feature was intrinsic to PG 1211+143, and not an artifact in COS, we examined the individual exposures in each FP-POS setting. The broad absorption feature appears in all four
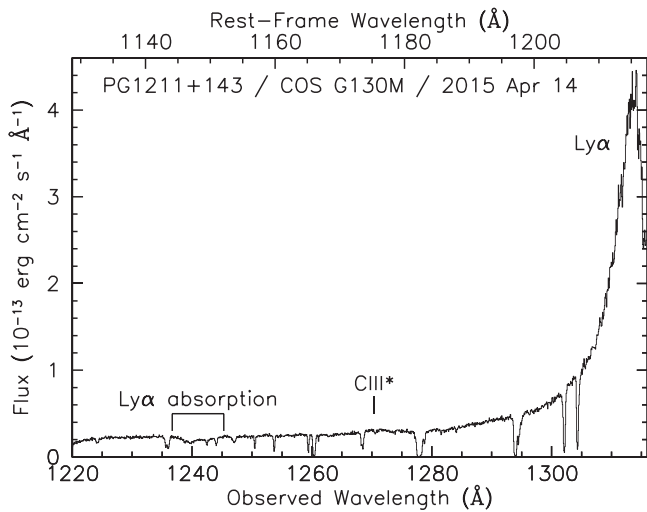
Figure 2. *HST*/COS G130M spectrum covering wavelengths in the blue wing of the Lyα emission line of PG 1211+143. The lower horizontal axis is the observed wavelength in ångstroms. The upper horizontal axis gives wavelengths in the rest frame of PG 1211+143 at $z = 0.0809$. The broad feature labeled "Lyα absorption" at an observed wavelength of 1240 Å is weak or absent in archival spectra. Emission lines of C III* λ1176 and Lyα in PG 1211+143 are labeled. All other narrow absorption lines arise in foreground interstellar or intergalactic gas.

exposures. Furthermore, no similar feature is present in any of the white dwarf standard star spectra obtained monthly as part of the COS calibration monitoring program.

To conclusively associate this single spectral feature with Lyα absorption intrinsic to PG 1211+143, we note the following: (1) If it were N V, one would expect to see Lyα at shorter wavelengths, and also C IV at longer wavelengths. No features are present at those expected wavelengths in our observations. (2) The velocity of this feature in the rest frame of PG 1211+143 matches the velocity of the detected soft X-ray absorption (Danehkar et al. 2018). (3) We also detect Lyβ as described later in this section.

To measure the strength of the Lyα absorption feature, we used `specfit` (Kriss 1994) in IRAF to model the surrounding continuum and line emission and the embedded ISM and IGM absorption lines. For the continuum, we used a reddened power law of the form $f_\lambda = 3.78 \times 10^{-14}$ $(\lambda/1000 \text{ Å})^{-0.779}$ erg cm^{-2} s^{-1} Å^{-1} with foreground Galactic extinction of $E(B - V) = 0.030$ (Schlafly & Finkbeiner 2011). We also included foreground damped Lyα absorption due to the ISM with a column density of $N_H = 2.588 \times 10^{20}$ cm^{-2} (Wakker et al. 2011). The Lyα emission line of PG 1211+143 was modeled using three Gaussian emission components. Their parameters are summarized in Table 2. For the narrow foreground ISM and IGM lines, we used individual Voigt profiles. Finally, for the broad intrinsic Lyα absorption, we modeled its profile using two blended Gaussians in negative flux in order to account for its asymmetric, uneven profile. Since the broad Lyα line is well resolved, we obtain a lower limit on the column density using the apparent optical depth method (Savage & Sembach 1991) by integrating over the normalized absorption profile. The measured properties of the broad Lyα absorber are summarized in Table 3. Here we give the properties of the individual components in our fit as well as the properties of the full blended trough.
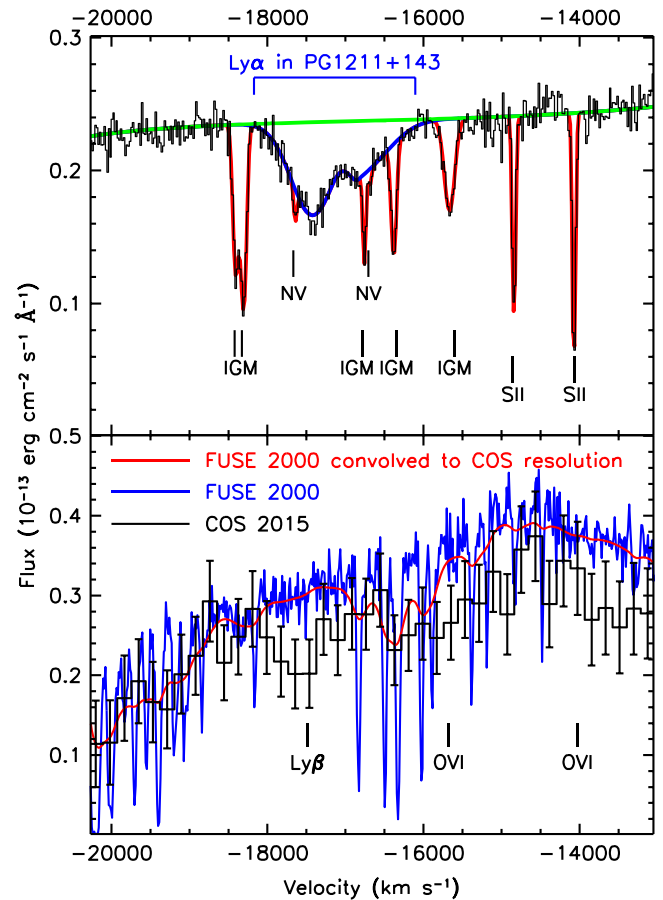
Figure 3. Upper panel: *HST*/COS G130M spectrum of PG 1211+143 in the wavelength region surrounding the broad Lyα absorption feature. The horizontal axis gives the outflow velocity relative to Lyα in the rest frame of PG 1211+143 at $z = 0.0809$. The blue line is our best-fit model for the broad Lyα absorption intrinsic to PG 1211+143. Intergalactic Lyα lines identified by Penton et al. (2004) are indicated by tick marks labeled "IGM." Interstellar lines of N V and S II are also labeled. The red line shows our best-fit model for these foreground absorption lines. The green line shows the emission model (continuum plus broad Lyα emission) with all absorption removed. Lower panel: COS and *FUSE* spectra of PG 1211+143 in the wavelength region corresponding to broad Lyβ absorption. The horizontal axis gives the outflow velocity relative to Lyβ in the rest frame of PG 1211+143 at $z = 0.0809$. The black histogram with 1σ error bars shows the COS G140L data, binned by 8 pixels. The blue line is the *FUSE* spectrum from 2000 (Tumlinson et al. 2005). All the absorption features in the *FUSE* spectrum are foreground interstellar absorption. The red line is the *FUSE* data convolved with the COS G140L line-spread function. Both the original *FUSE* data and the convolved spectrum are scaled to the intensity of the COS spectrum at 1040 Å. The expected minimum of Lyβ absorption that would correspond to the Lyα absorption trough is marked. The expected locations of O VI λλ1032, 1038 are also marked.

Since the short wavelength segment of our G140L grating observations covers the Lyβ region of PG 1211+143, we are also able to measure Lyβ absorption over the same velocity range as we see in Lyα. The spectrum in this observed wavelength range is more complex due to foreground Galactic ISM features and the lower resolution of the G140L grating. To aid in this analysis, we retrieved the archival *FUSE* observation of PG 1211+143 reported by Tumlinson et al. (2005). We convolved this with the COS G140L line-spread function (Roman-Duval et al. 2013) and scaled the flux level to match our COS spectrum at 1060 Å. The comparison shown in the lower panel of Figure 3 reveals a deficiency in flux in our COS spectrum relative to *FUSE* precisely at the wavelengths expected for a Lyβ counterpart to the G130M Lyα absorption

Table 2
Parameters of the Broad Emission Components in PG 1211+143

Line	λ_o (Å)	Flux (10^{-14} erg cm^{-2} s^{-1})	Velocity (km s^{-1})	FWHM (km s^{-1})
		STIS 2013		
C III*	1176.0	3.5 ± 0.3	-560 ± 44	1400 ± 130
Lyα	1215.67	9.6 ± 0.3	1240 ± 40	460 ± 170
Lyα	1215.67	33 ± 0.2	-170 ± 5	660 ± 10
Lyα	1215.67	280 ± 0.4	300 ± 5	2200 ± 10
Lyα	1215.67	110 ± 0.2	-1070 ± 5	3800 ± 30
Lyα	1215.67	250 ± 0.1	980 ± 5	13800 ± 22
		COS 2015		
C III*	1176.0	0.8 ± 0.3	-160 ± 190	860 ± 120
Lyα	1215.67	7.4 ± 0.9	-180 ± 17	330 ± 26
Lyα	1215.67	7.6 ± 1.2	20 ± 160	1000 ± 36
Lyα	1215.67	143 ± 1.8	-100 ± 5	1450 ± 14
Lyα	1215.67	142 ± 0.5	-470 ± 6	3600 ± 26
Lyα	1215.67	196 ± 1.5	860 ± 30	$13,100 \pm 33$

feature. We are not able to resolve the Lyβ absorption in the same detail as we can for Lyα, so we simply measure its integrated properties. If we use the scaled and convolved *FUSE* spectrum to normalize the COS spectrum and integrate this normalized spectrum over the velocity range -1500 to $+1500$ km s^{-1}, again using the apparent optical depth method of Savage & Sembach (1991), we obtain an equivalent width (EW) of 0.91 ± 0.27 Å. This flux deficiency is significant at a confidence level of >0.998 compared to the null hypothesis of no absorption. As shown in Table 3, the strength of the Lyβ absorption is comparable to that of Lyα, suggesting that both spectral features might be heavily saturated. This sets a lower limit on the H I column density of $N_H > 2.9 \times 10^{14}$ cm^{-2}. Given that the features are not black at the bottoms of the troughs, the H I absorption would then only partially cover the continuum source. To measure the covering fractions cited in Table 3, we use the depth at the center of the absorption trough. We note that since the Lyβ feature appears to be narrower than Lyα, this may indicate that the absorber is stratified in its column density, being more optically thick at line center than at higher velocities.

We do not see absorption associated with other high-ionization lines in the COS spectrum. No troughs associated with O VI, N V, or C IV are visible in our spectra. Although there appear to be deficiencies in flux in the COS spectrum at the expected locations of the O VI doublet in the lower panel of Figure 3, these are not statistically significant at more than 2σ confidence. Table 4 gives upper limits at 2σ confidence to the equivalent widths and column densities of these features assuming they have profiles similar to the detected Lyα absorption. The high saturation present in H I and this lack of associated high-ionization lines suggests that this absorbing gas is both very highly ionized and of high total column density.

Tumlinson et al. (2005) observed PG 1211+143 using a very deep (45 ks) STIS echelle E140M observation in 2002. We examined this archival spectrum to see if there was any indication of Lyα absorption at the velocity of our COS detection. Figure 4 compares the prior STIS observation of PG 1211+143 to our new COS observation. One can see a slight depression in the same region as the much more prominent absorption we have detected with COS. Although

this depression is marginally significant ($P > 0.96$ for the null hypothesis of no absorption), it is not an obvious feature one would have selected without knowing where to look in the spectrum. Its weakness (or even absence) in the prior STIS spectrum indicates that this H I absorption feature is variable in strength. The *HST*-Faint Object Spectrograph observation of PG 1211+143 in 1991 also bolsters this case for variability. Here we can set an upper limit on the presence of a Lyα absorption feature at $v_{out} = -16,980$ km $^{-1}$ comparable to the strength of that in the STIS spectrum.

Outflows at velocities of -3000 km s^{-1} and $-24,000$ km s^{-1} have also been reported in prior X-ray observations of PG 1211+143 (Pounds et al. 2003; Kaspi & Behar 2006). We have carefully examined our COS spectra in these velocity ranges. As shown in Table 4, we find no evidence for H I absorption at any velocity other than surrounding $-16,980$ km s^{-1}.

3. Discussion

Our joint *Chandra* and *HST* observations of PG 1211+143 clarify the confusing kinematics of at least one major outflow component in this important example of a UFO. The *HST*-COS detection of a broad Lyα absorption feature at an outflow velocity of $-16,980$ km s^{-1} ($0.0551c$) matches the velocity of the high-ionization absorption component detected in the joint *Chandra*-HETGS spectrum at $v_{out} = -17,300$ km s^{-1} ($z_{out} = -0.0561c$) (Danehkar et al. 2018). This absorber may be the same as the $-0.066c$ component detected in the deeper *XMM-Newton* EPIC-pn observation of Pounds et al. (2016). Analysis of the RGS data from the 2014 *XMM-Newton* observations (Reeves et al. 2017) reveals that this absorber has two components at velocities of $-0.062 \pm 0.001c$ ($v_{out} = -18,600 \pm 300$ km s^{-1}) and $-0.059 \pm 0.002c$ ($v_{out} = -17,700 \pm 600$ km s^{-1}), the latter of which is compatible with our detected H I absorption, but it has lower ionization, $\log \xi = 2.81$ compared to $\log \xi = 3.4$, and it is lower in column density, $N_H = 3 \times 10^{21}$ cm^{-2} compared to $N_H = 10 \times 10^{21}$ cm^{-2}.

The kinematics of the *Chandra* X-ray absorber detected by Danehkar et al. (2018) make it a good match to the *HST*-COS Lyα absorber reported in this paper. A crucial question, however, is whether the absorbing gas detected in our UV spectrum is identically the same gas as that seen in the *Chandra* spectrum with the exact same physical conditions. Fukumura et al. (2010) constructed a photoionization model of a magnetohydrodynamically accelerated UFO in which the high-ionization gas producing Fe XXV could also have associated UV absorption lines (C IV in particular). They find that producing detectable ionic concentrations of low-ionization species typical of UV spectra, e.g., C IV, in such high-ionization gas requires a fairly soft spectrum with a low X-ray to UV luminosity ratio. In their model, they require $\alpha_{ox} = 1.7$, which is characteristic of higher redshift, high-luminosity QSOs. In the $z = 3.912$ UFO source APM 08279 + 5255, which has $\alpha_{ox} = 1.7$, Hagino et al. (2017) successfully produce a model that includes both low-ionization UV absorption consistent with the broad UV absorption lines viewed in this object as well as lower-ionization X-ray absorption (compared to Fe XXV). In contrast, our *Chandra*+*HST* observations show that PG 1211+143 has a much higher X-ray to UV luminosity ratio, with an observed $\alpha_{ox} = 1.47$. Our best-fit photoionization model for the X-ray absorbing gas in Danehkar et al. (2018) predicts very low column densities for all commonly

Table 3
Properties of the Broad Lyα Absorption in PG 1211+143

Line	λ_ϱ (Å)	EW (Å)	Velocity (km s^{-1})	FWHM (km s^{-1})	C_f	log N_{ion} (log cm^{-2})	Predicted log N_{ion} (log cm^{-2})
			FOS 1991				
Lyα	1215.67	<0.45	−16,980	1080	1.0	<13.90	...
			STIS 2002				
Lyα	1215.67	0.45 ± 0.04	−17,450 ± 15	880 ± 10	0.1	<13.90	...
			COS 2015				
Lyα	1215.67	0.86 ± 0.12	−17,420 ± 15	653 ± 36	0.30 ± 0.04	>14.30	...
Lyα	1215.67	0.41 ± 0.17	−16,825 ± 36	320 ± 74	0.30 ± 0.04	>13.95	...
Lyα total	1215.67	1.27 ± 0.18	−16,980 ± 40	1080 ± 800	0.30 ± 0.04	>14.46	13.95
Lyβ	1025.72	0.91 ± 0.27	−17,464 ± 90	350 ± 50	0.33 ± 0.14	>15.20	13.95

observed UV metal ions (C IV, N V, and O VI). These predicted column densities are given in the last column of Table 4, and they are far below the upper limits for these ions that we measure in our *HST* spectra.

Although the ionic concentrations of the UV metal ions are extremely low, the predicted column density of H I is much higher due to its high abundance. Our best-fit photoionization model (Danehkar et al. 2018) predicts a neutral hydrogen column of 8.8×10^{13} cm^{-2}. This is lower than the lower limit derived from our Lyα measurement, $>2.9 \times 10^{14}$ cm^{-2}, but this prediction hinges crucially on the shape of the ionizing spectrum in the Lyman continuum. Our assumed spectral energy distribution is weighted toward a high ionizing luminosity since it extrapolates both the UV continuum and the soft X-ray continuum to a meeting point in the extreme ultraviolet (Figure 4 in Danehkar et al. 2018). However, a softer SED with a break to a steeper power law at the Lyman limit that then extrapolates to the detected soft X-ray continuum has half the ionizing flux in the Lyman continuum. Spectra with such a break are common in composite quasar spectra (Zheng et al. 1997; Telfer et al. 2002) and in the spectra of individual objects (Shang et al. 2005). With such a softer SED, the predicted neutral hydrogen column is 3.2×10^{14} cm^{-2}, which is compatible with our UV observation.

Alternatively, one could reconcile the lower predicted H I column density of the X-ray spectrum with the higher column density observed in Lyα if the X-ray absorber is associated with only a portion of the Lyα trough. As illustrated by our model in Figure 3 and the parameters in Table 3, the red component of the Lyα blend has a lower column density, compatible with the X-ray absorber. Its line width (FWHM $= 320 \pm 74$ km s^{-1}, $v_{turb} = 226 \pm 52$ km s^{-1}) is also a better match to the turbulent velocity inferred for the X-ray absorber, $v_{turb} = 91^{+205}_{-59}$ km s^{-1}.

Although the column densities of detected (H I) and undetected UV species are quite compatible with both the X-ray and UV absorption arising in the same gas, the complexity of the UV line profile relative to the X-ray may indicate that there are physically separate zones commingled in the outflow. Hagino et al. (2017) suggest that the UV-absorbing gas in APM 08279+5255 is due to higher-density clumps embedded in the X-ray UFO. This may be true in PG 1211

+143, but one would need higher S/N X-ray observations with better spectral resolution as well as higher S/N UV observations of the Lyβ and O VI region to resolve this possibility.

In contrast to the outflow at $v_{out} = -16,980$ km s^{-1} ($z_{out} = -0.0551$), seen with both *Chandra* and *HST*-COS, in neither observation do we detect the ultra-high-velocity gas at $-0.129c$ previously noted by Pounds et al. (2016). Pounds et al. (2016) cite multiple transitions of Fe XXV and Fe XXVI as evidence for this higher velocity gas. It has a total equivalent hydrogen column density of $N_H = (3.7 \pm 2.9) \times 10^{23}$ cm^{-2} at an even higher ionization parameter of log $\xi = 4.0$. For the PG 1211+143 spectral energy distribution in Danehkar et al. (2018), the fractional abundance of H I scales with ξ as log $N_{H I} = -3.47 - 1.4$ log ξ. Thus this $-0.129c$ gas component should have an associated neutral hydrogen column density of $\sim 3.1 \times 10^{14}$ cm^{-2}, which should be easily visible in a UV spectrum. Indeed, this is as strong as the Lyα absorption we detect that is associated with the lower-velocity, lower-ionization component of the outflow detected in our *Chandra* spectrum. At the location of a putative $-0.129c$ component in our COS spectrum, we can set an upper limit on any Lyα absorption of $<1.0 \times 10^{14}$ cm^{-2}, well below any expected absorption associated with such a component. At log $\xi = 3.4$ or 4.0, the trace columns of other UV-absorbing ions such as O VI, N V, or C IV would be $N_{ion} < 10^{13}$ cm^{-2} and undetectable in our COS spectra. Although we detect neither X-ray nor UV absorption associated with the high-velocity $-0.129c$ outflow, this could simply be due to variability, as even the H I counterpart of the $v_{out} = -17,300$ km s^{-1} ($z_{out} = -0.0561$) X-ray absorber is not always detectable, as shown in Figure 4.

While we do not confirm all of the ultrafast outflow components previously seen in PG 1211+143, we do have a robust detection of one at an outflow velocity of $v_{out} = -16,980$ km s^{-1} ($z_{out} = -0.0551$). However, this outflow component is considerably lower in total column density than previously suggested features. Is it then massive enough and energetic enough to have a substantive impact on the evolution of its host galaxy? As usual, this is still ambiguous since derivation of the mass outflow rate and the kinetic luminosity depend on the location of the absorbing gas we have detected. The further from the central source, the more massive the

Table 4
Upper Limits for Absorption Features in PG 1211+143

Line	λ_o (Å)	EW (Å)	Velocity (km s^{-1})	FWHM (km s^{-1})	log $N_{\rm ion}$ (log cm^{-2})	Predicted log $N_{\rm ion}$ (log cm^{-2})
O VI	1032,1038	<0.62	−16,980	1080	<14.51	12.83
N V	1238,1242	<0.12	−16,980	1080	<13.58	10.72
C IV	1548,1550	<0.22	−16,980	1080	<13.56	8.91
Lyα	1215.67	<0.17	−3000	1080	<13.50	...
Lyα	1215.67	<0.074	−24,000	1080	<13.13	...
Lyα	1215.67	<0.53	−38,700	1080	<14.00	14.49
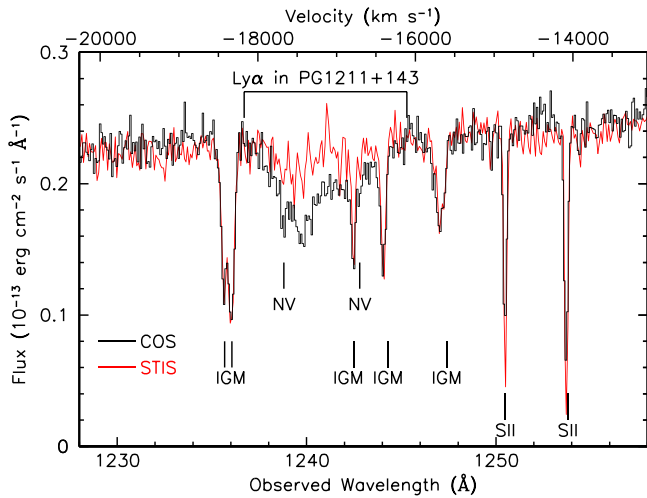
Figure 4. Comparison of the STIS E140M spectrum of PG 1211+143 to the *HST*/COS G130M spectrum in the region around the broad Lyα absorption feature shows that the absorption feature has varied. The red line is the STIS data binned by 6 pixels; the black histogram is the COS spectrum binned by 8 pixels. The lower horizontal axis is the observed wavelength in ångstroms. The upper horizontal axis gives the outflow velocity of Lyα in the rest frame of PG 1211+143 at $z = 0.0809$. Interstellar and intergalactic lines are labeled as in Figure 3.

outflow, and the higher its kinetic luminosity. Assuming the outflow is in the form of a partial thin spherical shell moving with velocity v, its mass flux, $\dot{M}$, and kinetic luminosity, $\dot{E}_k$, are given by

$$\dot{M} = 4\pi \Delta\Omega R N_{\rm H} \mu m_p v$$

$$\dot{E}_k = \frac{1}{2}\dot{M}v^2,$$

where $\Delta\Omega$ is the fraction of the total solid angle occupied by the outflow, R is the distance of the outflow from the central source, $N_{\rm H}$ is the total hydrogen column density of the outflow, $m_{\rm p}$ is the mass of the proton, and $\mu = 1.4$ is the molecular weight of the plasma per proton. Since Tombesi et al. (2010) argues that roughly 50% of AGNs have ultrafast, high-ionization outflows, we assume $\Delta\Omega = 0.5$.

As many authors have argued, the maximum radius can be estimated by assuming a plasma of uniform density distributed along the line of sight to the central source, so that $N_{\rm H} = nR$ (e.g., Blustin et al. 2005; Reeves & Pounds 2012; Ebrero et al. 2013). Given that we know the ionization parameter $\xi = L_{\rm ion}/(nR^2)$, this gives the constraint $R < L_{\rm ion}/(N_{\rm H}\xi)$. For our observation of PG 1211+143 and the SED presented by Danehkar et al. (2018), $L_{\rm ion} = 1.587 \times 10^{45}$ erg s^{-1}. $N_{\rm H} = 3 \times 10^{21}$ cm^{-2} and $v = 16,980$ km s^{-1}, so that $R < 265$ pc, $\dot{M} < 799\,M_\odot$ yr^{-1} and

$\dot{E}_k < 7.3 \times 10^{46}$ erg s^{-1}. Our SED for PG 1211+143 gives a bolometric luminosity of 5.3×10^{45} erg s^{-1}, so at this maximum distance the outflow would be depositing up to $14\times$ the bolometric luminosity as mechanical energy into the host galaxy. This even exceeds the Eddington luminosity of 1.8×10^{46} erg s^{-1} for its black hole mass of $1.46 \times 10^8\,M_\odot$ (Peterson et al. 2004). However, given the unrealistic assumption involved in this approximation (i.e., a single ionization parameter describes gas uniformly distributed from 0 to 265 pc), this merely demonstrates the potentially powerful influence of this outflow on the host galaxy.

At the other extreme, if we assume the gas is a thin spherical shell at the radius where its velocity equals the escape velocity of its central black hole, for $v = 16,980$ km s^{-1}, $R = 5$ lt-day, the impact is minimal, with a mass outflow rate of $>0.013\,M_\odot$ yr^{-1}, and a kinetic luminosity of $>1.2 \times 10^{42}$ erg s^{-1}.

If the absorbing cloud is associated with an ejection event in 2001, we can set a better-motivated constraint on the location of the absorber. Variability in the Lyα absorption feature argues for changes related to motion of the absorber rather than an ionization response due to the magnitude of the variability. The observed changes in strength (from absence, or near-absence) from the prior FOS and STIS observations to our COS observation are much stronger than expected based on changes in the luminosity of PG 1211+143. In the archival record, PG 1211+143 spans a range in UV brightness at 1464 Å from 2.0×10^{-14} erg cm^{-2} s^{-1} Å^{-1} to 4.6×10^{-14} erg cm^{-2} s^{-1} Å^{-1} (Dunn et al. 2006). The FOS and STIS observations bracket this range with flux levels of 2.1×10^{-14} erg cm^{-2} s^{-1} Å^{-1} and 4.6×10^{-14} erg cm^{-2} s^{-1} Å^{-1}, respectively. Our COS observation lies near the lower end at 2.4×10^{-14} erg cm^{-2} s^{-1} Å^{-1}. For our adopted SED (Figure 4 in Danehkar et al. 2018), a factor of 2 change in flux translates to a factor of 2.5 change in the neutral hydrogen column density. Given the saturation present in Lyα in our COS spectrum, the column density has increased by more than a factor of 3.5. This bolsters the case that the X-ray/UV outflow is not continuous. It could either have originated as an ejection event around 2001, or it could imply that the absorbing cloud is moving transverse to our line of sight.

For motion at −16,980 km s^{-1}, an ejected cloud would have moved outward to a distance of 7×10^{17} cm (0.23 pc) over 13 years. A thin spherical shell at this distance would imply a mass outflow rate of $>0.013\,M_\odot$ yr^{-1}, and a kinetic luminosity of 6×10^{43} erg s^{-1}. It is interesting to observe that this is more similar to the minimum kinetic luminosity of $>3 \times 10^{44}$ erg s^{-1} we derived for a potential radio jet based on the VLA observations (Danehkar et al. 2018), which appears energetically similar to the X-ray/UV outflow.

Unfortunately, none of these estimates are definitive since we have no good measurement of the actual location and duration of the outflow. With so few spectral diagnostics, pinning down the radius of such an outflow would require intensive monitoring to measure recombination timescales in the photoionized gas.

4. Summary

We have obtained high S/N UV spectra of the QSO PG 1211+143, covering the 900–1800 Å bandpass simultaneously with a deep *Chandra* X-ray observation (Danehkar et al. 2018). Our ultraviolet spectra detect a fast, broad Lyα absorption feature outflowing at a velocity of $v_{out} = -16,980 \, \mathrm{km \, s^{-1}}$ ($z_{out} = -0.0551$) with an FWHM of $1080 \, \mathrm{km \, s^{-1}}$. A possible feature associated with Lyβ is also detected at 99.8% confidence, but no other ionic species are detected in absorption at this velocity. This H I absorption feature is a likely counterpart of the highly ionized warm absorber detected in our *Chandra* HETGS spectrum at an outflow velocity of $v_{out} = -17,300 \, \mathrm{km \, s^{-1}}$ ($z_{out} = -0.0561$). This ultrafast outflow may be the same as the $v_{out} \sim -0.06c$ outflow reported in previous *XMM-Newton* observations by Pounds et al. (2016) and Reeves et al. (2017). Our detection of H I absorption associated with these outflows demonstrates that neutral hydrogen is a very sensitive tracer of high-column density gas even at high ionization.

ORCID iDs

Gerard A. Kriss ✪ https://orcid.org/0000-0002-2180-8266
Ashkbiz Danehkar ✪ https://orcid.org/0000-0003-4552-5997
Michael A. Nowak ✪ https://orcid.org/0000-0001-6923-1315
Taotao Fang ✪ https://orcid.org/0000-0002-2853-3808
Martin J. Hardcastle ✪ https://orcid.org/0000-0003-4223-1117
Joseph Neilsen ✪ https://orcid.org/0000-0002-8247-786X

References

Blustin, A. J., Page, M. J., Fuerst, S. V., Branduardi-Raymont, G., & Ashton, C. E. 2005, A&A, 431, 111
Borguet, B. C. J., Arav, N., Edmonds, D., Chamberlain, C., & Benn, C. 2013, ApJ, 762, 49
Crenshaw, D. M., & Kraemer, S. B. 2012, ApJ, 753, 75
Crenshaw, D. M., Kraemer, S. B., & George, I. M. 2003, ARAA, 41, 117
Danehkar, A., Nowak, M. A., Lee, J. C., et al. 2018, ApJ, 853, 165
Danforth, C. W., & Shull, J. M. 2008, ApJ, 679, 194
De Rosa, G., Peterson, B. M., Ely, J., et al. 2015, ApJ, 806, 128
Di Matteo, T., Springer, V., & Hernquist, L. 2005, Natur, 433, 604
Dunn, J. P., Jackson, B., Deo, R. P., et al. 2006, PASP, 118, 572
Ebrero, J., Kaastra, J. S., Kriss, G. A., de Vries, C. P., & Costantini, E. 2013, MNRAS, 435, 3028
Faucher-Giguère, C.-A., & Quataert, E. 2012, MNRAS, 425, 605
Ferrarese, L., & Merritt, D. 2000, ApJL, 539, L9
Fukumura, K., Kazanas, D., Contopoulos, I., & Behar, E. 2010, ApJL, 723, L228
Gallo, L. C., & Fabian, A. C. 2013, MNRAS, 434, L66
Gebhardt, K., Bender, R., Bower, G., et al. 2000, ApJL, 539, L13
Green, J. C., Froning, C. S., Osterman, S., et al. 2012, ApJ, 744, 60
Hagino, K., Done, C., Odaka, H., Watanabe, S., & Takahashi, T. 2017, MNRAS, 468, 1442
Hopkins, P. F., & Elvis, M. 2010, MNRAS, 401, 7
Kaspi, S., & Behar, E. 2006, ApJ, 636, 674
King, A. 2003, ApJL, 596, L27
King, A., & Pounds, K. 2015, ARA&A, 53, 115
Kriss, G. 1994, in ASP Conf. Ser. 61, Astronomical Data Analysis Software and Systems III, ed. D. R. Crabtree, R. J. Hanisch, & J. Barnes (San Francisco, CA: ASP), 437
Kriss, G. A., Arav, N., Kaastra, J. S., et al. 2011, A&A, 534, A41
Laha, S., Guainazzi, M., Dewangan, G. C., Chakravorty, S., & Kembhavi, A. K. 2014, MNRAS, 441, 2613
Liu, G., Zakamska, N. L., & Greene, J. E. 2014, MNRAS, 442, 1303
Liu, G., Zakamska, N. L., Greene, J. E., Nesvadba, N. P. H., & Liu, X. 2013a, MNRAS, 430, 2327
Liu, G., Zakamska, N. L., Greene, J. E., Nesvadba, N. P. H., & Liu, X. 2013b, MNRAS, 436, 2576
Ostriker, J. P., Choi, E., Ciotti, L., Novak, G. S., & Proga, D. 2010, ApJ, 722, 642
Penton, S. V., Stocke, J. T., & Shull, J. M. 2004, ApJS, 152, 29
Peterson, B. M., Ferrarese, L., Gilbert, K. M., et al. 2004, ApJ, 613, 682
Pounds, K., Lobban, A., Reeves, J., & Vaughan, S. 2016, MNRAS, 457, 2951
Pounds, K. A., & Reeves, J. N. 2009, MNRAS, 397, 249
Pounds, K. A., Reeves, J. N., King, A. R., et al. 2003, MNRAS, 345, 705
Reeves, J., Lobban, A., & Pounds, K. 2017, ApJ, submitted (arXiv:1801.03784)
Reeves, J., & Pounds, K. 2012, in ASP Conf. Ser. 460, AGN Winds in Charleston, ed. G. Chartas, F. Hamann, & K. M. Leighly (San Francisco, CA: ASP), 13
Roman-Duval, J., Elliott, E., Aloisi, A., et al. 2013, COS/FUV Spatial and Spectral Resolution at the new Lifetime Position, Tech. Rep Instrument Science Report, COS 2013-07
Savage, B. D., & Sembach, K. R. 1991, ApJ, 379, 245
Schlafly, E. F., & Finkbeiner, D. P. 2011, ApJ, 737, 103
Shang, Z., Brotherton, M. S., Green, R. F., et al. 2005, ApJ, 619, 41
Silk, J., & Rees, M. J. 1998, A&A, 331, L1
Soker, N. 2010, MNRAS, 407, 2355
Telfer, R. C., Zheng, W., Kriss, G. A., & Davidsen, A. F. 2002, ApJ, 565, 773
Thompson, T. A., Fabian, A. C., Quataert, E., & Murray, N. 2015, MNRAS, 449, 147
Tilton, E. M., Danforth, C. W., Shull, J. M., & Ross, T. L. 2012, ApJ, 759, 112
Tombesi, F., & Cappi, M. 2014, MNRAS, 443, L104
Tombesi, F., Cappi, M., Reeves, J. N., et al. 2010, A&A, 521, A57
Tombesi, F., Cappi, M., Reeves, J. N., et al. 2011, ApJ, 742, 44
Tumlinson, J., Shull, J. M., Giroux, M. L., & Stocke, J. T. 2005, ApJ, 620, 95
Vaughan, S., & Uttley, P. 2008, MNRAS, 390, 421
Wakker, B. P., Lockman, F. J., & Brown, J. M. 2011, ApJ, 728, 159
Zheng, W., Kriss, G. A., Telfer, R. C., Grimes, J. P., & Davidsen, A. F. 1997, ApJ, 475, 469
Zoghbi, A., Miller, J. M., Walton, D. J., et al. 2015, ApJL, 799, L24
Zubovas, K., & Nayakshin, S. 2014, MNRAS, 440, 2625